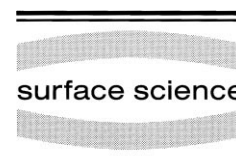




ELSEVIER

Surface Science 442 (1999) L983–L988



www.elsevier.nl/locate/susc

Surface Science Letters

Enhanced oxidation rate of Ni(111) by atomic oxygen

J.A. Slezak, B.D. Zion, S.J. Sibener *

The James Franck Institute and Department of Chemistry, The University of Chicago, 5640 South Ellis Avenue, Chicago, IL 60637, USA

Received 27 July 1999; accepted for publication 24 August 1999

Abstract

The oxidation of the Ni(111) surface by a supersonic atomic oxygen beam has been quantitatively studied using in situ high-resolution electron-energy-loss spectroscopy. For a room temperature substrate, a drastically different oxidation rate is observed for atomic oxygen induced oxidation than for molecular oxygen based oxidation. This rate was found to be two orders of magnitude higher than that for molecular oxygen. The reaction on a 110 K substrate indicated oxygen uptake only to the chemisorption saturate, with no further oxidation. This later finding agrees with previous results for low surface temperature oxidation using molecular oxygen, implying that the inhibiting step in low temperature Ni oxidation is not molecular oxygen dissociation, but a more fundamental property of the metallic substrate. The chemisorption region of the atomic oxygen reaction was found to saturate at the same sub-monolayer as results from exposure to molecular oxygen, i.e. a dense (1×1) overlayer as has been seen on other metals does not form on Ni(111). © 1999 Published by Elsevier Science B.V. All rights reserved.

Keywords: Atom–solid interactions; Electron energy loss spectroscopy (EELS); Molecule–solid reactions; Nickel; Nickel oxides; Oxidation; Oxygen; Surface chemical reaction

Understanding the oxidation of metals is of great interest in both the areas of corrosion and catalysis. Nickel has traditionally been one of the metals used to test new concepts in oxidation, and has been the focus of many oxidation studies [1–12]. It is of particular interest because it is highly resistant to metallic oxidation and corrosion.

Oxidation of metals by atomic oxygen is of particular interest. In the upper atmosphere there is a relatively high concentration of atomic oxygen, and it is not known how it reacts with various satellites and aircraft traveling in that region of the atmosphere [13,14]. J.S. Brodtkin et al. placed

nickel wafers in earth orbit, resulting in a 350 Å thick, porous NiO layer [15]. However, no detailed study in a controlled UHV system has been performed.

In this Letter, the interaction of atomic oxygen with a room temperature and a relatively low temperature (110 K) nickel surface is addressed. Through the use of high-resolution electron-energy-loss spectroscopy (HREELS), we observed the rate of the room temperature reaction of atomic oxygen to be two orders of magnitude greater than that of molecular oxygen. No difference was observed in the cold substrate.

Other aspects of the chemisorption region for atomic oxygen reacting with Ni(111) were also investigated. It has recently been observed that a

* Corresponding author. Fax: +1-773-702-5863.

E-mail address: s-sibener@uchicago.edu (S. Sibener)

dense (1×1) oxygen overlayer can be obtained on both Rh and Ru. The reaction of molecular oxygen and Rh(111) saturates at a half monolayer coverage, a $p(2 \times 1)$ overlayer structure. Atomic oxygen dosing can induce a dense, full monolayer coverage having a (1×1) oxygen overlayer structure [16]. This is supported by theoretical work that predicted a dense oxygen overlayer to be thermodynamically stable [17,18]. Both a dense, (1×1) oxygen overlayer, formed by dissociative NO_2 dosing, and a 0.75 ML oxygen overlayer, formed by O_2 dosing, have been formed on Ru [19,20]. The dense (1×1) overlayer has also been examined theoretically [21]. As shown in this Letter, this dense overlayer is not seen for atomic oxygen interacting with Ni(111).

A great deal is known about the interaction of molecular oxygen and nickel. Holloway and Hudson have characterized three regions of oxide growth, the initial fast chemisorption stages, a fast oxide growth stage, and a slow oxide growth stage. They have found that the fast oxide growth stage is very dependent on nucleation site formation [7,8]. In previous work from our group, it was

found that electron bombardment induces oxidation at 120 K, whereas oxide does not form in the presence of molecular oxygen alone at this temperature [1–3]. Work done by Zion et al. found that high kinetic energy beams can also affect the mechanism of oxide formation [4]. In this Letter, it is shown that the use of atomic oxygen as a reagent greatly increases the rate of metallic oxidation.

The apparatus, described elsewhere [4], consists of a two-level UHV chamber. The upper level consists of an argon ion sputtering gun, an Auger spectrometer, and low energy electron diffraction (LEED). The lower level consists of an LK2000 HREELS, a three-stage molecular-beam source, and a Quadrupole Mass Analyzer (QMA) (Fig. 1). The molecular-beam source is oriented at 15° from the surface normal of the crystal, and is aligned such that its spot coincides with the HREELS spot on the crystal. The sample used is a Ni(111) crystal, as described in detail elsewhere [1–3]. Surface preparation consisted of argon ion sputtering the Ni(111) crystal for 10 min, followed by annealing at 1100 K for 10 min.

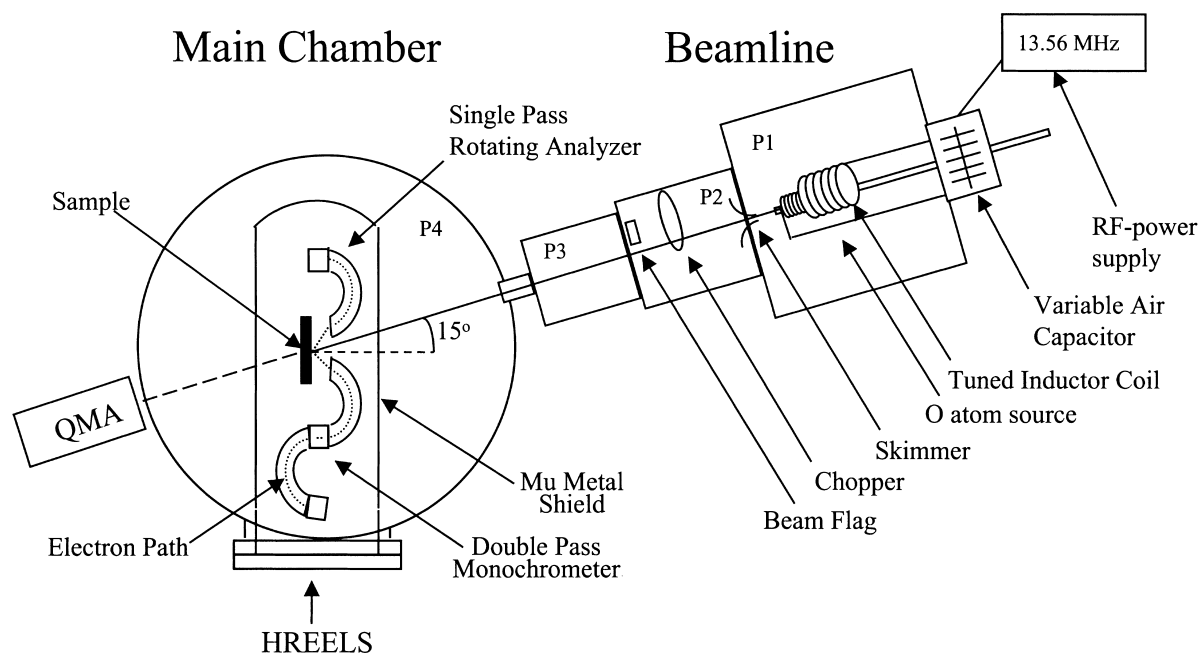


Fig. 1. Schematic of the experimental arrangement used in this study. P1, P2, P3, and P4 denote different differentially pumped regions.

An atomic oxygen beam source was constructed according to the design specifications of Sibener et al. [13]. An OEM-6 RF-power supply was used with a frequency of 13.56 MHz and output powers ranging from 0 to 650 W; the nozzle diameter was 80 μm . The gas mixture used was 5% O_2 in He. Typical conditions for the plasma were 150 Torr backing pressure and a RF-power of 100 W. The resulting atomic oxygen beam was primarily $\text{O}(^3\text{P}_1)$ with a minor constituent of $\text{O}(^1\text{D}_2)$, with a kinetic energy of 150 meV and a 30% dissociation rate of the O_2 , measured by time of flight analysis. The flux of the O_2 beam was found to be 0.5 Langmuirs (L), obtained by overlapping molecular oxygen reaction data over previously acquired molecular oxygen reaction data of Zion et al. [4], and extrapolating the flux of the current beam. Atomic oxygen fluxes were taken to be 30% of the molecular oxygen beam flux.

Sample dosing and HREELS acquisition were conducted alternately. Total dosing time for the atomic oxygen runs was typically up to 2.5 h, and for molecular oxygen it was extended to 8 h due to lower reactivity. In each case, this was the time necessary to reach saturation of the reaction.

Oxygen uptake versus coverage curves for both atomic and molecular oxygen were obtained in a similar manner to that of Zion et al. [4]. The ratio of the integrated area of the HREELS oxide peak to the integrated area of the specular peak, normalized to 3 ML total coverage, was plotted against the exposure in Langmuirs, yielding the oxidation curve.

Fig. 2 shows the typical oxidation curve for room temperature atomic oxygen dosing compared with that for molecular oxygen dosing. The atomic oxygen curve has a similar shape to that of the molecular oxygen curve. It is again characterized by three regions, the fast chemisorption stage, the fast oxide growth stage, and the slow oxide saturation stage, as delineated by Holloway and Hudson [7,8]. The data has been fit with two different models, the island growth model of Holloway and Hudson, and the Langmuir model of Zion et al. [4], which will be described in detail later. Based on fitting statistics, it is inconclusive as to which model best fits the data. Therefore, we have chosen

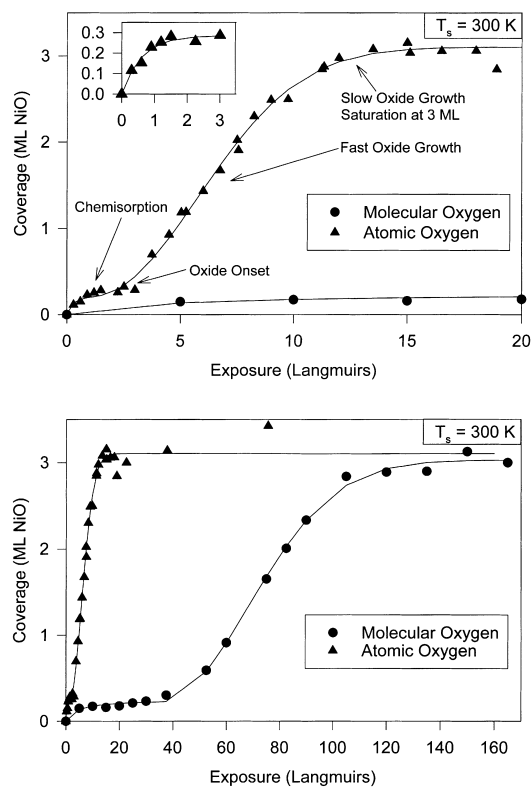


Fig. 2. (a) Low exposure view of the atomic oxygen and molecular oxygen induced oxidation curve. Inset is the expanded view of the chemisorption region of the atomic oxygen induced oxidation curve, with a sticking coefficient of 0.9. The triangles represent the atomic oxygen oxidation curve, and the circles represent the molecular oxygen oxidation curve. Lines represent the fits of the island growth model to the data. The characteristic regimes of oxidation have been labeled. (b) Longer-time data for oxygen uptake versus exposure for both atomic and molecular oxygen.

the more widely used island growth model for most of the analyses presented herein.

The island growth model assumes the lateral growth of oxide islands. Parameters in the model include the number of initial nucleation sites, as well as the rate of collisions of the oxygen molecules/atoms and the rate constant for perimeter growth. The rate expression, modified from Holloway and Hudson, is as follows:

$$\Theta(\Phi) = \Theta_{\text{sat}} - (\Theta_{\text{sat}} - \Theta_{\text{chem}}) \exp[-KN_0(\Phi - \Phi_0)^2],$$

for $\Phi > \Phi_0$,

where Θ_{sat} is the saturation coverage, taken to be 3 ML [1,2], Θ_{chem} is the chemisorption saturation, Φ_0 is the oxide onset exposure, N_0 is the number of nucleation sites, and K is the rate of perimeter growth. This expression is valid only in the oxidation region. The rate of perimeter growth, K , and the number of nucleation sites, N_0 , are not separable parameters in this model. The average composite rate parameter of atomic oxygen oxidation, KN_0 , was found to be $0.026 \pm 0.003 \text{ L}^{-2}$.

The Langmuir model has a first-order dependence on exposure. It assumes that the oxidation growth rate depends on the impingement rate of the oxygen atoms/molecules, a Langmuir surface coverage dependence, and a rate constant. The derived oxidation rate expression is as follows:

$$\Theta(\Phi) = \Theta_{\text{sat}} - (\Theta_{\text{sat}} - \Theta_{\text{chem}}) \exp[-K(\Phi - \Phi_0)],$$

for $\Phi > \Phi_0$.

The average rate constant for oxidation, K , that was found for this model was $0.20 \pm 0.04 \text{ L}^{-1}$.

Fit parameters of the island growth model to the atomic oxygen data and the molecular oxygen data are given in Table 1. The parameters given for molecular oxygen oxidation are for the data set given in this paper. This value is consistent with previous values found for molecular oxygen oxidation [4]. The differences between the molecular and atomic oxygen oxidation curves lie in differing rates of reaction. *Atomic oxygen induced oxidation occurs about 100 times faster than that for molecular oxygen induced oxidation in all regimes of oxygen uptake.* This agrees with work done by Raspopov et al. with a polycrystalline nickel ribbon [5]. They studied resistance changes,

not under controlled UHV conditions, as a function of atomic oxygen coverage at high temperatures (773–1373 K). Their findings implied reaction rates several orders of magnitude greater than that of molecular oxygen oxidation.

This great increase in the rate can be explained by the high reactivity of atomic oxygen. Molecular oxygen must catalytically dissociate in order to chemisorb on the surface and subsequently create oxide. With atomic oxygen, a bond does not need to be broken at the surface, giving 498 kJ/mol additional energy to the reactants [22]. The rate of the atomic oxygen reaction is unambiguously much faster.

An interesting parameter that can be extracted from the data is the sticking coefficient. This parameter gives the rate that the impinging atoms stick to the surface. For the room temperature reaction of atomic oxygen oxidation, it was found to be 0.9, as compared to 0.23 for molecular oxygen [23]. Therefore, it can be concluded that almost every oxygen atom that hits the surface chemisorbs to the surface.

Atomic oxygen impinging on a cold crystal (110 K) did not induce deep metallic oxidation. Fig. 3a shows the comparison of atomic oxygen dosing on a room temperature substrate and a 110 K substrate. These data show conclusively that atomic oxygen does not induce oxidation at 110 K. To further confirm this result, we initially dosed the crystal with molecular oxygen, which has been shown not to oxidize low temperature nickel, but rather reach saturation at a chemisorbed overlayer [1–3]. The crystal was then subsequently dosed with atomic oxygen and monitored for additional oxidation (Fig. 3b). The amount of oxygen on the surface did not change, indicating no further metallic oxidation [1–3]. After the incident oxygen atoms have equilibrated with the metal surface, they are not capable of low temperature bulk oxidation. Either more energy needs to be added than the energy of the O_2 bond, perhaps in the form of higher kinetic energies, or an additional stimulant needs to be added, as in the electron stimulated oxidation of Stirniman et al. [1–3]. These results imply that molecular oxygen dissociation is not the inhibiting step in low temperature

Table 1
Parameters of the Island Growth Model fit to both the molecular and atomic oxygen induced oxidation^a

	O_2	O
KN_0	$4.7 \times 10^{-4} \text{ O}_2 \text{ L}^{-2}$	$0.026 \pm 0.003 \text{ L}^{-2}$
Θ_{sat}	2.8 ML	$2.8 \pm 0.1 \text{ ML}$
Φ_0	36 L	$0.7 \pm 0.6 \text{ L}$

^a KN_0 = rate constant times initial number of nucleation sites; Θ_{sat} = saturation thickness of oxide; Φ_0 = exposure at onset of oxidation.

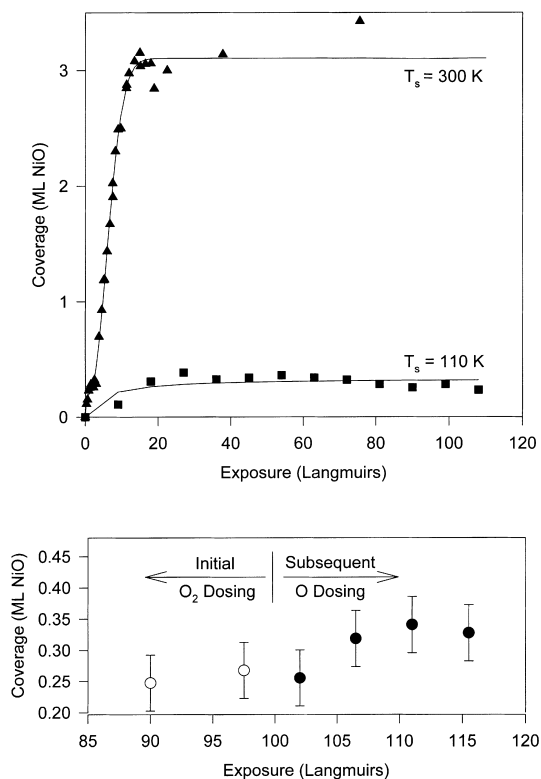


Fig. 3. (a) Oxygen uptake versus exposure for both the room temperature and cold temperature reactions of atomic oxygen. (b) Oxygen uptake versus exposure for cold substrate temperature dosing of molecular oxygen followed by dosing of atomic oxygen. Open circles denote molecular oxygen dosing, and solid circles denote atomic oxygen dosing.

Ni oxidation, but a more fundamental property of the metallic substrate.

We have also examined whether dosing with atomic oxygen could lead to the formation of a dense, high-coverage (1×1) oxygen chemisorbed overlayer on Ni(111). The reaction of molecular oxygen with Ni(111) results in a $p(2 \times 2)$ overlayer of chemisorbed O at room temperature. In Fig. 2 it can be seen that in the room temperature atomic oxygen reaction, the chemisorption overlayer reaches the 0.25 ML coverage, just as in the molecular oxygen reaction. Also, in the cold temperature reaction, where no oxide is formed, we see little to no additional oxygen on the surface (Fig. 3). When we look with LEED at low temperature Ni(111) which has been exposed to atomic oxygen, no

ordered overlayer is seen, just as for dosing with molecular oxygen. Note that this result is different from that of Rh [16–18] and Ru [19,20], where a dense oxygen overlayer can be formed. The smaller relative lattice spacing for Ni(111) (2.49 Å) [24] as compared with the values for Rh(111) (2.69 Å) and Ru(0001) (2.71 Å) [24] may well be the reason that a dense (1×1) overlayer does not form at either room temperature or under cryogenic conditions.

In summary, we have examined the oxidation of Ni(111) with atomic oxygen, and compared it with that of molecular oxygen at both room and cold temperatures. It was determined that the rate of room temperature oxidation using atomic oxygen, primarily $O(^3P_j)$, has a rate two-orders of magnitude higher than that characteristic of molecular oxygen. Atomic oxygen does not, however, induce deep metallic oxidation at cryogenic temperatures (110 K). Also, a dense oxygen overlayer is not formed in the chemisorption region of the reaction of atomic oxygen on Ni(111), unlike Rh(111) or Ru(0001).

These results indicate that fundamental issues persist as we seek to develop a truly predictive understanding of metallic oxidation, especially when dealing with highly energetic oxidants. Molecular beam experiments, supported by accurate electronic structure calculations and scattering theory, are now poised to answer these longstanding issues in interfacial chemistry.

Acknowledgements

This work was supported by the Air Force Office of Scientific Research (AFOSR with AASERT augmentation) and, in part, by the MRSEC Program of the National Science Foundation at The University of Chicago, Award No. DMR-9808595.

References

- [1] M.J. Stirniman, L. Wei, S.J. Sibener, J. Chem. Phys. 103 (1995) 451.

- [2] L. Wei, M.J. Stirniman, S.J. Sibener, *J. Vac. Sci. Technol. A* 13 (1995) 1574.
- [3] L. Wei, M.J. Stirniman, S.J. Sibener, *Surf. Sci.* 329 (1995) L593.
- [4] B.D. Zion, A.T. Hanbicki, S.J. Sibener, *Surf. Sci.* 417 (1998) L1154.
- [5] S.A. Raspopov, A.G. Gusakov, A.G. Voropayev, A.A. Vecher, B.K. Grishin, *J. Alloys Compounds* 227 (1995) 5.
- [6] W.-D. Wang, N.J. Wu, P.A. Thiel, *J. Chem. Phys.* 92 (1990) 2025.
- [7] P.H. Holloway, J.B. Hudson, *Surf. Sci.* 43 (1974) 123.
- [8] P.H. Holloway, J.B. Hudson, *Surf. Sci.* 43 (1974) 141.
- [9] P.H. Holloway, *J. Vac. Sci. Technol.* 18 (1981) 653.
- [10] A. Atkinson, D.W. Smart, *J. Electrochem. Soc.* 135 (1998) 2886.
- [11] O.L. Warren, P.A. Thiel, *J. Chem. Phys.* 100 (1994) 659.
- [12] C.R. Brundle, J.Q. Broughton, in: A. King, D.P. Woodruff (Eds.), *The Chemical Physics of Solid Surfaces and Heterogeneous Catalysis* vol. 3, part A, Elsevier, Amsterdam, 1990, pp. 132–388, and references cited therein.
- [13] S.J. Sibener, R.J. Buss, C.Y. Ng, Y.T. Lee, *Rev. Sci. Instrum.* 51 (1980) 167.
- [14] P.N. Peters, H.C. Gregory, J.T. Swann, *Appl. Opt.* 25 (1986) 1290.
- [15] J.S. Brodtkin, L.C. Sengupta, W. Franzen, P.L. Sagalyn, *Thin Solid Films* 234 (1993) 512.
- [16] K.D. Gibson, M. Viste, E.C. Sanchez, S.J. Sibener, *J. Chem. Phys.* 110 (1999) 2757.
- [17] E.J. Walter, S.P. Lewis, A.M. Rappe, in preparation.
- [18] M.V. Ganduglia-Pirovano, M. Scheffler, *Phys. Rev. B* 59 (1999) 15533.
- [19] C. Stampfl, S. Schwegmann, H. Over, M. Scheffler, G. Ertl, *Phys. Rev. Lett.* 77 (1996) 3371.
- [20] K.L. Kostov, M. Gsell, P. Jakob, T. Moritz, W. Widdra, D. Menzel, *Surf. Sci.* 394 (1997) L138.
- [21] C. Stampfl, M. Scheffler, *Phys. Rev. B* 54 (1996) 2868.
- [22] P.W. Atkins, *Physical Chemistry*, 5th ed., W.H. Freeman, New York, 1994.
- [23] J.T. Stuckless, C.E. Wartnaby, N. Al-Sarraf, J.B. Dixon-Warren, M. Kovar, D.A. King, *J. Chem. Phys.* 106 (1997) 2021.
- [24] D.R. Lide (Ed.), *CRC Handbook of Chemistry and Physics*, 72nd ed., CRC Press, Boston, 1991.